

# Study of linearity for a high dynamic range calorimeter<sup>\*</sup>

XIANG Tian(项天)<sup>1;1)</sup> JIN Xi(金西)<sup>2;2)</sup> DONG Jia-Ning(董家宁)<sup>1</sup> ZHANG Yun-Long(张云龙)<sup>2</sup>  
 XU Zi-Zong(许咨宗)<sup>2</sup> LIU Shu-Bin(刘树彬)<sup>2</sup> An Qi(安琪)<sup>2</sup>

<sup>1</sup> Department of Physics, University of Science and Technology of China, Hefei 230026, China

<sup>2</sup> Department of Modern Physics, University of Science and Technology of China, Hefei 230026, China

**Abstract:** A high dynamic range calorimeter has been designed for the DArk Matter Particles Explore (DAMPE) satellite. It consists of 308 BGO crystals, multi-dynode readout PMTs and front end electronics system. We have built on previous research to show that BGO fluorescence should not be saturated by high electron energy density under DAMPE's energy range. A BGO fluorescence simulator is set up to calibrate the energy range of the dynodes, while a cosmic-ray unit is used to calibrate 1 MIP with the ADC count in dynode 8. Linearity is achieved for the dynamic range from 0.5 MIPs to  $1.26 \times 10^5$  MIPs. The requirements of DAMPE can thus be satisfied.

**Key words:** DAMPE, BGO calorimeter, PMT, LED, high dynamic

**PACS:** 29.40.Vj, 29.85.-c **DOI:** 10.1088/1674-1137/38/4/046201

## 1 Introduction

A high-energy particle passing through a scintillation crystal causes excitation of electrons in the crystal, which leads to fluorescence when the electron decays back to its ground state. By measuring the fluorescence energy, the energy deposited by the incident particle can be inferred.

Current cosmological models now include an invisible dark matter, which is inferred from gravitational effects on visible matter. According to the theoretical models, when dark matter particles annihilate, high energy electrons will be generated [1]. By making use of PMTs to detect fluorescence where generated by high-energy electrons passing through a BGO calorimeter, the DArk Matter Particles Detection satellite (DAMPE) can infer the existence of dark matter [2].

BGO crystal is the main functional component of the calorimeter. BGO ( $\text{Bi}_4\text{Ge}_3\text{O}_{12}$ ) is a colorless, high density crystal, with good chemical stability and high mechanical strength, and it does not dissolve in water or organic solvents. The fluorescence intensity of BGO crystal has a linear relationship with the energy deposited by incident particles. The highest intensity of the fluorescence emission spectrum is near 480 nm, which allows easy spectral matching with PMTs [3].

The main component of the BGO calorimeter is 308 pieces of BGO crystal, stacked into a framework of 14 layers.

The size of each BGO crystal is 2.5 cm×2.5 cm×60 cm.

A PMT (R5611 from Hamamatsu) is placed on one side of each BGO crystal. The BGO calorimeter response energy should vary from 5 GeV to 10 TeV, which is far beyond the CERN maximum energy limitation of 290 GeV. In simulations, the maximum value of the deposited energy in a crystal is about 1.7 TeV for electrons of 10 TeV, and a dynamic readout range from 0.5 MIPs (about 11.5 MeV) to  $1 \times 10^5$  MIPs (about 1.7 TeV) should be available [4, 5].

For achieving a high dynamic range readout measurement, a Hamamatsu PMT R5611 is coupled with a BGO bar to read out the fluorescence from dynodes 2, 5 and 8, which correspond to high, medium and low energy ranges. In this paper, we will first explain the fluorescence saturation of the BGO crystal, we will then present an experiment to prove the linearity of the readout system.

## 2 BGO crystal fluorescence saturation

Generally, when the ionization density in an organic crystal is high, a fluorescence saturation effect that can be described by Birks' Law will occur. However, there is not yet an accurate model for fluorescence saturation in inorganic crystals, such as BGO. We have developed a model of the BGO calorimeter using the simulation software GEANT4, with the parameters given above, with which we successfully detected and analyzed electrons of

Received 6 May 2013, Revised 29 August 2013

<sup>\*</sup> Supported by Strategic Priority Research Program of Chinese Academy of Science (XDA04040202-4)

1) E-mail: xt860706@mail.ustc.edu.cn

2) E-mail: jinxi@ustc.edu.cn

©2014 Chinese Physical Society and the Institute of High Energy Physics of the Chinese Academy of Sciences and the Institute of Modern Physics of the Chinese Academy of Sciences and IOP Publishing Ltd

high energy (5–10 TeV). It can be seen from the simulation that the average maximum energy deposition in a crystal is 1.7 TeV when electrons of energy 10 TeV pass through the BGO calorimeter as part of an electromagnetic shower. The energy deposition within a cylinder of radius 2.23 cm and height 2.5 cm is about 1.5 TeV (1.7 TeV×90%), while the Moliere radius of BGO crystal is 2.23 cm, which is smaller than the expected 2.5 cm. The average density of energy deposition is then about 5 GeV/mm<sup>3</sup>. Using these simulation results, we must now consider whether or not the fluorescence saturation effect occurs in the BGO crystal.

The Northwest Institute of Nuclear Technology have previously researched the fluorescence saturation effect using the pulsed gamma radiation device “Qiangguang-1”, using high dose rates in LSO crystal [6]. It shows that the light output is linear when the fluence rate of the pulsed gamma radiation is no more than  $1.9 \times 10^{19}$  MeV/(cm<sup>2</sup>·s). In this situation, the bulk density of the energy absorption per cubic millimeter reaches up to 7000 TeV/mm<sup>3</sup>, which is far higher than that in the shower center (5 GeV/mm<sup>3</sup>). Consequently, it is reasonable to believe that electrons of 10 TeV energy in BGO crystal, which is also an inorganic crystal, will not lead to the fluorescence saturation effect and that the light output will be linear. In addition, the final state particles produced in the electromagnetic shower are mostly low-LET (linear energy transfer) electrons. Therefore, it is reasonable to expect that the fluorescence quenching effect will not occur in BGO crystal in our experiment [4].

### 3 BGO fluorescence simulator

Since no electron beam could cover such a wide energy range, a BGO fluorescence simulator was set up to calibrate the energy range of the dynodes, as shown in Fig. 1. The BGO fluorescence simulator consists of a pulse generator (GEN), a control unit (CTRL), an LED, and one of several integrating spheres (ISP).

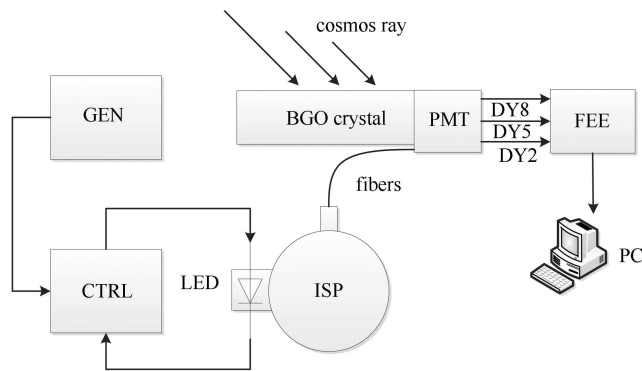


Fig. 1. Schematic diagram of BGO fluorescence simulator.

The details of the setup are as follows.

1) An AFG3252 from Tektronix was used as a pulse generator. Its output range supports from 50 mV to 5 V, accurate to 1 mV.

2) The control unit controls the current through the LED, making sure that current is proportional to the pulse generator output.

3) Light scattered by the interior of the integrating sphere is evenly distributed over all angles [7–9]. Several optical fibers are used to transmit the light; intensity is proportional to the cross section of the fiber.

4) A BGO crystal is connected to the PMT to measure cosmic rays and to calibrate the dynodes to 1 MIP.

### 3.1 LED comparison and choice

The cathode sensitivity of the Hamamatsu R5611 PMT is in the range 450 nm to 500 nm [10], so an LED in that range should be chosen. A SSP6612 type LED optics and electricity parameter tester was used to measure peak wavelengths and luminosity for a range of possible LEDs. Table 1 shows the various LEDs and their peak wavelengths, while Fig. 2 shows the current-flux curve.

Table 1. Possible LEDs with their peak wavelengths.

company	model	peak wavelength/nm
Bivar	3UBWC-0.6	464.2
Kingbright	WP7113QBC	464.9
Dialight	521-9946F	467.2
Avago	HLMP-CB14_UX	464.2
Optek	OVLGB0C6B9	466.6
CREE	C503B-BAS-CY0462	468.3

From Fig. 2 it is clear that all LEDs tend to saturate with current increase. The Optek OVLGB0C6B9 shows the best performance, so it was chosen as the light source of the simulator.

### 3.2 Control unit

A schematic of the control unit is shown in Fig. 3.  $V_i$  is the input signal and  $D_1$  is the operating load.

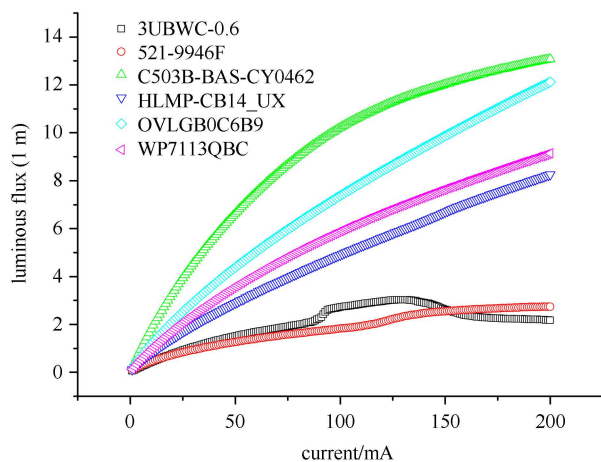


Fig. 2. Current-flux curves for LEDs under consideration.

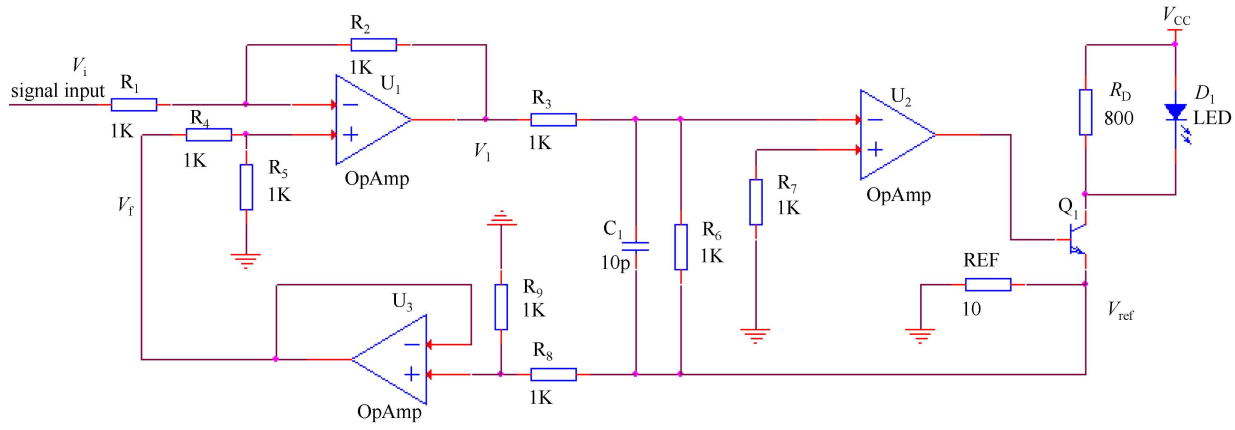


Fig. 3. Schematic of control circuit.

The op-amp U1 and resistors R1, R2, R4, R5 constitute a subtracter:

$$V_1 = V_f - V_i. \quad (1)$$

The output of U2 is controlled by  $V_1$ , which changes the current in the collector of transistor Q1, and then affects the feedback voltage  $V_{ref}$ :

$$V_{ref} = I_E \cdot R_{ref}, \quad (2)$$

$$V_1 = V_f - V_i. \quad (3)$$

U3, R8 and R9 constitute a divider:

$$V_f = \frac{1}{2} V_{ref}. \quad (4)$$

Combining Eqs. (1)–(4), it can be found that:

$$I_E = \frac{2}{3} \frac{V_i}{R_{ref}}. \quad (5)$$

Therefore, the output current is proportional to the input voltage.

The performance of the BGO fluorescence simulator is also dependent on  $R_D$ . A smaller  $R_D$  gives a lower pedestal current (the current through the LED when  $V_i$  equal to 0) and poorer linearity when the current through the LED is low.

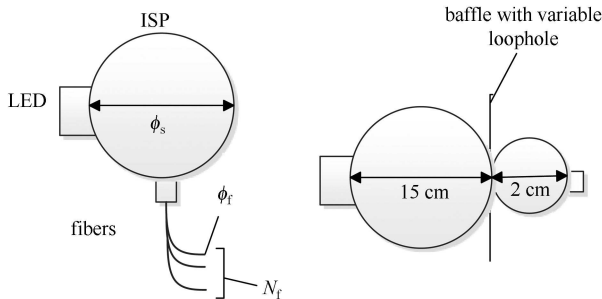


Fig. 4. Schematic of integrating sphere system.

### 3.3 Integrating sphere

Since the output of the simulator should cover three dynodes, as well as guarantee precision at low intensity, different kind of ISPs and fibers have been used to adjust the energy range of the PMT. Fig. 4 shows the ISP and fiber system. A detailed description of the ISPs is given in the next section.

## 4 Experiment and results

### 4.1 Experimental method

To prove the linearity of dynodes DY2, DY5 and DY8, while measuring the dynamic range of the calorimeter, the BGO fluorescence simulator was used. A series of measurements of different parameters was done to obtain the full response of the BGO calorimeter, since

- 1) The main range of the BGO fluorescence simulator shows good linearity; and,
- 2) The dynamic range of the BGO calorimeter is too large to allow the whole range to be covered in only one measurement.

The system was tested with six different configurations, as shown in Table 2. In Table 2,  $\phi_s$  is the diameter of the ISP,  $\phi_f$  is the diameter of the fiber,  $N_f$  is the number of fibers,  $S_b$  is the area of the loophole in the baffle, and  $R_{ref}$  is the reference resistance of the control unit.

The experimental method was then as follows:

- 1) Select one of the configurations shown in Table 2.

Table 2. Simulator configurations.

index	$\phi_s/\text{mm}$	$\phi_f/\text{mm}$	$N_f$	$S_b/\text{mm}^2$	$R_{ref}/\Omega$	$R_D/\Omega$
a	60	0.5	3	N.A.	19	596
b	60	0.5	3	N.A.	187.2	9.98 k
c	150	0.3	1	N.A.	31.6	10 k
d	150+20	0.3	1	N.A.	33	10 k
e	150+20	0.3	1	2	33	10 k
f	150+20	0.3	1	10	33	10 k

2) Regulate the voltage of the signal source, and record the ADC count of the 3 PMT dynodes.

3) Calculate the current through the LED according to the formula for the voltage and current in the control circuit.

4) Repeat steps 2) and 3) for the whole range of the signal generator.

5) Select another of the configurations in step 1) and repeat the above steps until the three dynode outputs of the PMT are all at their maxima.

### 4.2 Results

The results of the six configuration tested are shown in Fig. 5, where the  $x$  axis shows the output flux of the LED, not the flux received by the PMT, and the  $y$  axis shows the ADC count of the three dynodes with the pedestal subtracted.

Since there is a well-known relationship between the ADC count of the dynodes and the photon flux received by the PMT, sample points from one of the configuration plots above can be transferred to any of the other plots, using the relationship of the LED flux in the different configurations.

It can be calculated that the linear fit function for the first configuration (Fig. 5) is

$$y = \alpha kx, \tag{6}$$

where  $y$  is the ADC count,  $x$  is the output flux of the LED,  $\alpha$  is the flux attenuation coefficient for the first con-

figuration, and  $k$  is the cathode sensitivity of the PMT.

For the second plot, that function is

$$y = \beta kx, \tag{7}$$

where  $\beta$  is the flux attenuation coefficient for the second configuration.

We can multiply the  $x$  axis of Equation 6 by  $\beta/\alpha$ , giving

$$y = \alpha kx \cdot \frac{\beta}{\alpha} = \beta kx. \tag{8}$$

The two plots can then be combined. However, it is hard to find the flux attenuation coefficient, so a compromise method is to make the slopes of the two functions coincident.

For example, we stretch the  $x$  axis in Fig. 5(a) (Fig. 6(a)) to make the slope as same as that of Fig. 5(b), then combine Fig. 5(b) and Fig. 6(b) to get Fig. 6(c). The black line shown in Fig. 6(c) then represents the whole response of DY2, and the  $x$  axis shows the equivalent flux for Configuration b (Con. b).

Figure 7 shows the combination of all six figures in the same way, where the ‘standard unit’ shown on the  $x$  axis is the equivalent flux of Con. c, and the ADC count on the  $y$  axis is that of the three dynodes with the pedestal subtracted. Using the cosmic ray measurement device shown in Fig. 1 for calibration, 1 MIP corresponds to an ADC count of 106 for DY8, which corresponds to a Standard Unit of 0.0475. The maximum output of DY2

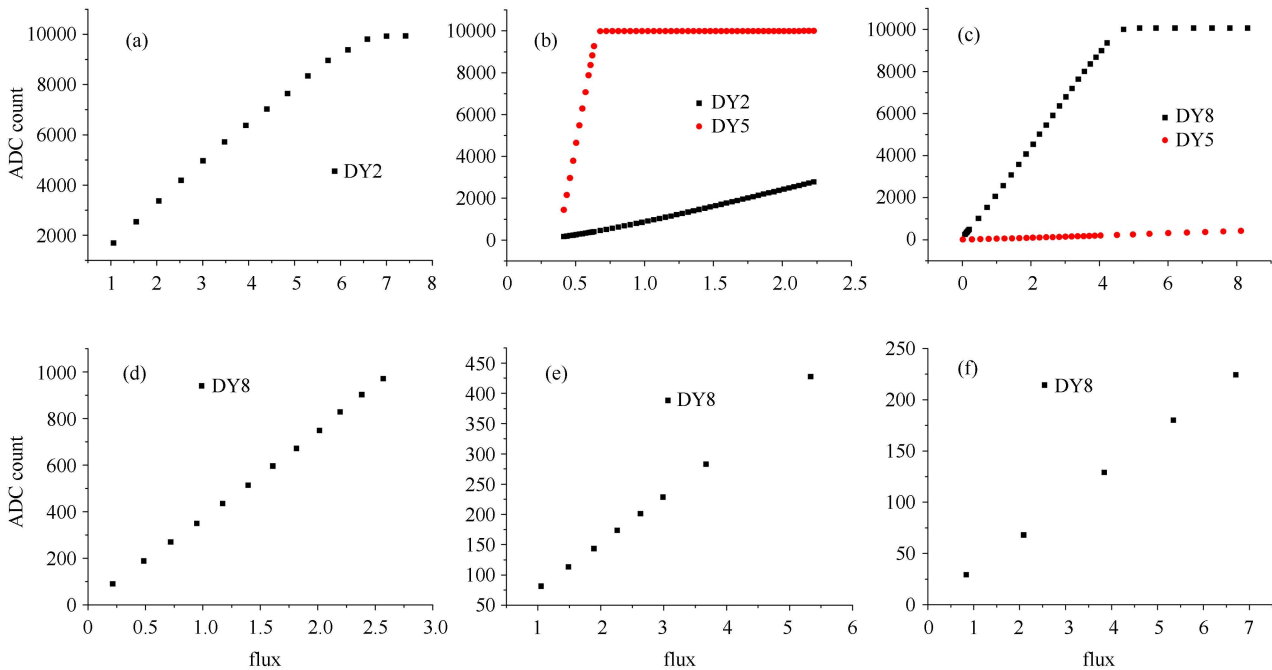


Fig. 5. Dependence of ADC count on LED output flux for each configuration.

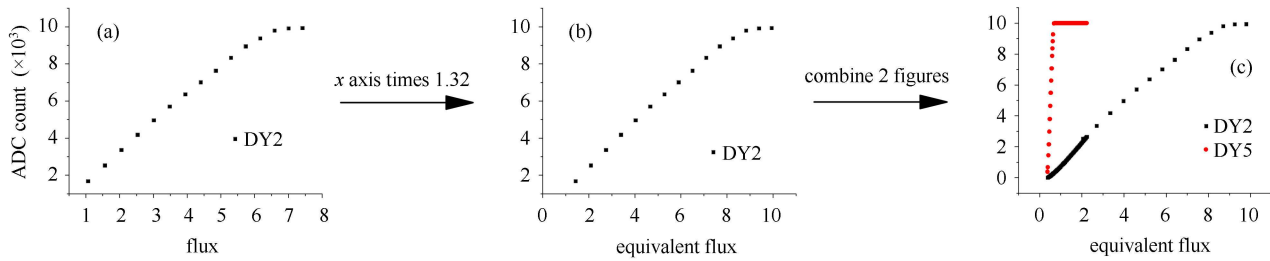


Fig. 6. Strategy for combining results from different configurations.

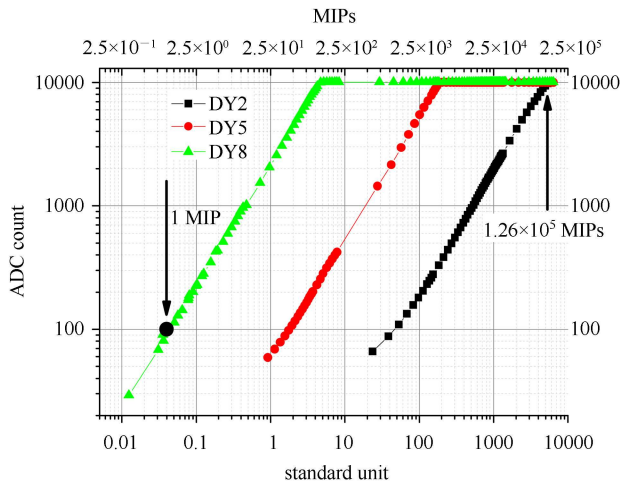


Fig. 7. Calibration results for PMT.

shown in Fig. 7 is 5990 Standard Units, corresponding to an ADC count of 9939 and  $1.26 \times 10^5$  MIPs.

## 5 Conclusion

In this paper, we discussed the requirements for the PMT which will be used in DAMPE and presented a large dynamic range BGO fluorescence simulator to prove the linearity of the PMT. The simulator consists of electronic units and optical units. The electronic units can generate a current pulse to make the optical units flash like a real BGO fluorescence. The optical units can decay the light intensity to increase the dynamic range.

In the simulator measurement, we changed the parameters of electronic units and optical units, and created six different configurations. Since the six configurations gave us six dependent plots, we combined the six plots into one plot based on the relationship of LED flux in the different configurations and the features of the PMT.

After the simulator measurement, we used the cosmic ray measurement device for calibration, mark 1 MIP at the combined plot, the dynamic range is shown to be able to cover a range from 0.5 to  $1.26 \times 10^5$  MIPs.

## References

- 1 CHANG J. *Journal of Engineering Studies*, 2010, **2**(2): 95–99
- 2 ZHANG Y L. *The Study of an EM Calorimeter for Searching Dark Matter in Space*. Dissertation for doctor's degree. University of Science and Technology of China, 2011
- 3 LIAO J Y, YE C Z, YANG P Z. *Chemical Research*, 2004, **15**(4): 52–58
- 4 ZHANG Y L, LI B, FENG C Q et al. *Chinese Physics C (HEP & NP)*, 2012, **36**(1): 71–73
- 5 FENG C Q. *The Research on the Readout Electronics for the Calorimeter Detector of the Dark Matter Exploration Satellite*. Dissertation for doctor's degree. University of Science and Technology of China, 2011
- 6 GUAN X Y, ZHANG Z C, ZHANG W Y. *Atomic Energy Science and Technology*, 2009, **43**(10): 942–945 (in Chinese)
- 7 LIU H X, SUN J X, LIU Z X et al. *Optics and Precision Engineering*, 2012, **20**(7): 1447–1454
- 8 WANG S R, XING J, LI F T. *Optics and Precision Engineering*, 2006, **14**(2): 185–190
- 9 CHEN F, YUAN Y L, XHENG X B et al. *Optics and Precision Engineering*, 2008, **16**(11): 2060–2064
- 10 HAMAMATSU. *Photomultiplier Tubes R5611*, [http://sales.hamamatsu.com/assets/pdf/parts\\_R/R5611.pdf](http://sales.hamamatsu.com/assets/pdf/parts_R/R5611.pdf)